J. Fluid Mech. (2021), *vol*. 928, R3, doi:10.1017/jfm.2021.840

Purely elastic linear instabilities in parallel shear flows with free-slip boundary conditions

Martin Lellep[1],†, Moritz Linkmann[2], Bruno Eckhardt[3],‡ and Alexander Morozov[1]

[1]SUPA, School of Physics and Astronomy, The University of Edinburgh, James Clerk Maxwell Building, Peter Guthrie Tait Road, Edinburgh EH9 3FD, UK

[2]School of Mathematics and Maxwell Institute for Mathematical Sciences, University of Edinburgh, Edinburgh, EH9 3FD, UK

[3]Physics Department, Philipps-University of Marburg, D-35032 Marburg, Germany

(Received 6 August 2021; revised 16 September 2021; accepted 21 September 2021)

We perform a linear stability analysis of viscoelastic plane Couette and plane Poiseuille flows with free-slip boundary conditions. The fluid is described by the Oldroyd-B constitutive model, and the flows are driven by a suitable body force. We find that both types of flow become linearly unstable, and we characterise the spatial structure of the unstable modes. By performing a boundary condition homotopy from the free-slip to no-slip boundaries, we demonstrate that the unstable modes are directly related to the least stable modes of the no-slip problem, destabilised under the free-slip situation. We discuss how our observations can be used to study recently discovered purely elastic turbulence in parallel shear flows.

Key words: polymers, viscoelasticity, shear-flow instability

1. Introduction

Stability of parallel shear flows of dilute polymer solutions is an outstanding problem of mechanics of complex fluids. While linear stability analyses performed with model viscoelastic fluids suggest that these flows are linearly stable (Gorodtsov & Leonov 1967; Wilson, Renardy & Renardy 1999), it has been proposed that they can lose their stability through a finite-amplitude, sub-critical bifurcation (Morozov & van Saarloos 2005, 2007, 2019), similarly to their Newtonian counterparts (Grossmann 2000). Recent experiments performed in pressure-driven straight channels support this scenario: for sufficiently high flow rates, there exists a critical strength of flow perturbations required to destabilise the

† Email address for correspondence: martin.lellep@ed.ac.uk
‡ Deceased on 7 August 2019.

flow (Pan *et al.* 2013), thus demonstrating the sub-critical nature of the transition. Beyond the transition, the flow exhibits features of purely elastic turbulence (Bonn *et al.* 2011; Pan *et al.* 2013; Qin & Arratia 2017), previously reported only in geometries with curved streamlines (Groisman & Steinberg 2000; Steinberg 2021).

Despite recent progress, the exact origin of purely elastic turbulence remains unknown. One of the major obstacles in understanding its mechanism is the absence of direct numerical simulations of confined flows at sufficiently high flow rates, due to the high Weissenberg number problem (Owens & Phillips 2002), which is of purely numerical origin. Although significant progress has been made in developing numerical methods capable of controlling this problem (Alves, Oliveira & Pinho 2021), direct numerical simulations relevant to experiments in parallel shear flows (Bonn *et al.* 2011; Pan *et al.* 2013; Qin & Arratia 2017) are still lacking. Here, we propose to circumvent the high Weissenberg number problem by studying parallel shear flows with free-slip boundary conditions that remove steep near-wall velocity gradients and significantly improve numerical stability.

The influence of wall slip on hydrodynamic stability of various flows has been extensively studied. The motivations behind these studies can be separated into two broad classes. The studies from the first class seek to approximate microscopically sound boundary conditions and thus address the question of linear stability of experimentally realisable flows. Such an approach has indicated, for instance, that the classical two-dimensional Tollmien–Schlichting transition in plane channel flow of Newtonian fluids is significantly suppressed by the presence of wall slip (Gersting 1974; Lauga & Cossu 2005; Min & Kim 2005), although the non-normal energy growth mechanism was shown to be less affected (Lauga & Cossu 2005). When adapted to shear flows of polymeric fluids, this approach revealed the existence of a short-wavelength instability (Black & Graham 1996, 1999, 2001), which is absent in the corresponding no-slip flows.

The second class of studies employs slip boundary conditions exclusively as the means to simplify the underlying no-slip boundary condition problem. The free-slip boundary conditions usually adopted in these works are rather artificial, yet they yield significantly more tractable mathematical problems. This approach was pioneered by Rayleigh (1916) in the context of Rayleigh–Bénard instability. More recently, Waleffe (1997) used free-slip boundary conditions to construct exact coherent states in parallel shear flows of Newtonian fluids that revolutionised our understanding of the transition to turbulence in those flows (Eckhardt *et al.* 2007; Tuckerman, Chantry & Barkley 2020; Graham & Floryan 2021). The most important outcome of these studies is the observation that free-slip systems preserve the main phenomenology of their no-slip counterparts, albeit at increased values of the control parameter. Our work draws its motivation from this class of studies.

Here, we perform a linear stability analysis of plane Couette flow (pCF) and pressure-driven plane Poiseuille flow (pPF) with free-slip boundary conditions. We employ the Oldroyd-B model (Bird, Armstrong & Hassager 1987) in the absence of inertia, and demonstrate numerically that these flows develop linear instabilities absent in their no-slip counterparts. Importantly, we observe that the main features of no-slip flows are preserved under the free-slip conditions, and we discuss how these instabilities can be employed to gain insight into the nature of elastic turbulence in parallel geometries.

2. Problem set-up

We study incompressible flows of a model viscoelastic fluid confined between two infinite parallel plates. We introduce a Cartesian coordinate system $\{x_1, x_2, x_3\}$ oriented along the

streamwise, gradient and spanwise directions, respectively; the plates are located at $x_2 = \pm L$. The dynamics of the fluid is assumed to be described by the Oldroyd-B model (Bird *et al.* 1987),

$$\boldsymbol{\tau} + Wi\left[\frac{\partial \boldsymbol{\tau}}{\partial t} + \boldsymbol{v}\cdot\boldsymbol{\nabla}\boldsymbol{\tau} - (\boldsymbol{\nabla}\boldsymbol{v})^{\mathrm{T}}\cdot\boldsymbol{\tau} - \boldsymbol{\tau}\cdot(\boldsymbol{\nabla}\boldsymbol{v})\right] = (\boldsymbol{\nabla}\boldsymbol{v}) + (\boldsymbol{\nabla}\boldsymbol{v})^{\mathrm{T}}, \tag{2.1a}$$

$$Re\left[\frac{\partial \boldsymbol{v}}{\partial t} + \boldsymbol{v}\cdot\boldsymbol{\nabla}\boldsymbol{v}\right] = -\boldsymbol{\nabla}p + \beta\boldsymbol{\nabla}^2\boldsymbol{v} + (1-\beta)\boldsymbol{\nabla}\cdot\boldsymbol{\tau} + \boldsymbol{f}, \tag{2.1b}$$

$$\boldsymbol{\nabla}\cdot\boldsymbol{v} = 0, \tag{2.1c}$$

where $\boldsymbol{v}$, $\boldsymbol{\tau}$ and p are the fluid velocity, the polymeric Cauchy stress tensor and the pressure, respectively, while $(\boldsymbol{\nabla}\boldsymbol{v})^{\mathrm{T}}$ denotes the transpose of the velocity gradient tensor; $\boldsymbol{f}$ is a body force to be specified below. These equations are rendered dimensionless using the channel's half-width L as the unit of length, the maximum velocity of the laminar profile V_0 as the unit velocity, and L/V_0 as the unit of time. The governing equations (2.1) feature three dimensionless groups, the Weissenberg number $Wi = \lambda V_0/L$, the Reynolds number $Re = \rho L V_0/\eta$ and the viscosity ratio $\beta = \eta_s/\eta$, where λ is the Maxwell relaxation time of the fluid, ρ is its density, and η_s and η are the solvent viscosity and the total viscosity of the fluid, respectively. Unless stated otherwise, below we focus on the purely elastic limit with $Re = 0$.

The fluid is assumed to satisfy the following free-slip boundary conditions at the walls:

$$\partial_2 v_1 = v_2 = \partial_2 v_3 = 0, \quad \text{for } x_2 = \pm 1, \tag{2.2}$$

where ∂_2 denotes the spatial derivative in the gradient direction. In this work, we study unidirectional laminar profiles $\boldsymbol{v} = \{U(x_2), 0, 0\}$, where U is chosen to resemble the shape and symmetry of either plane Poiseuille flow (pPF) or plane Couette flow (pCF), while satisfying the boundary conditions (2.2):

$$U(x_2) = \begin{cases} \sin(\pi x_2/2) & (\text{pCF}), \\ \cos(\pi x_2/2)^2 & (\text{pPF}). \end{cases} \tag{2.3}$$

The corresponding laminar components of the polymeric stress tensor are given by $\tau_{11} = 2Wi(\partial_2 U(x_2))^2$ and $\tau_{12} = \partial_2 U(x_2)$, with all other components being zero. To drive such flows in the presence of free-slip boundary conditions, we add the body force $\boldsymbol{f} = \{-\partial_2^2 U(x_2), 0, 0\}$ to the right-hand side of (2.1*b*).

To perform a linear stability analysis of these flows, we linearise the equations (2.1) around the laminar profile given above. In view of the viscoelastic analogue of Squire's theorem (Bistagnino *et al.* 2007), which also holds for the free-slip boundary conditions studied here, we consider two-dimensional modal perturbations $\{\delta\boldsymbol{v}(x_2), \delta\boldsymbol{\tau}(x_2), \delta p(x_2)\}\,\mathrm{e}^{\mathrm{i}k_1 x_1}\,\mathrm{e}^{\sigma t}$ of the velocity, stress and pressure, respectively. Here, k_1 sets the spatial scale of the perturbation, and $\sigma = \sigma_r + i\sigma_i$ denotes a complex temporal eigenvalue, with σ_r and σ_i being its real and imaginary part, respectively. The x_2 dependences of the perturbations are expanded in Chebyshev polynomials, and the linearised equations of motion are solved with a fully spectral Chebyshev–Tau method (Canuto *et al.* 1987) by employing the generalised eigenvalue solver eig from the scientific library SciPy for Python (Virtanen *et al.* 2020).

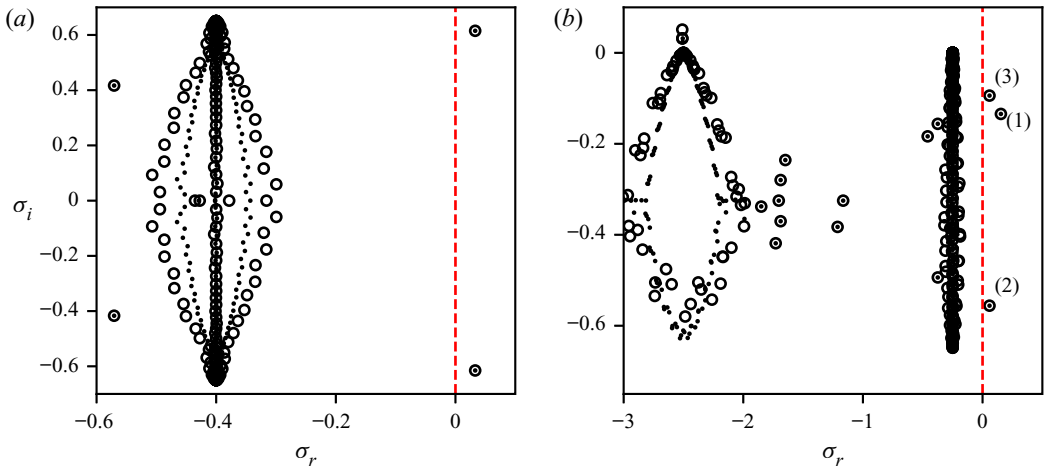

Figure 1. Eigenvalue spectra for $\beta = 0.1$ and $k_1 = 0.65$ for (*a*) pCF at $Wi = 2.5$, and (*b*) pPF at $Wi = 4.0$. The dashed red lines denote marginal stability. Both figures compare spectra calculated with 50 (open circles) and 100 (dots) Chebyshev polynomials.

3. Results

The no-slip pCF and pPF of Oldroyd-B fluids are linearly stable for a wide range of β and Wi (Gorodtsov & Leonov 1967; Wilson *et al.* 1999). Recently Khalid, Shankar & Subramanian (2021*b*) reported a purely elastic linear instability in no-slip pPF; however, its region of existence is confined to a small and, most likely, experimentally inaccessible part of the parameter space with $\beta > 0.9$ and $Wi > O(10^3)$. Surprisingly, here we find that free-slip pCF and pPF are linearly unstable for a wide range of β and Wi.

In figure 1, we present examples of such instabilities by plotting the eigenvalue spectra for pCF and pPF. Similarly to those of the no-slip problem (Wilson *et al.* 1999), the spectra consist of discrete physical eigenvalues and two lines of eigenvalues corresponding to continuous spectra with $\sigma_r = -1/Wi$ and $\sigma_r = -1/(\beta Wi)$; the finite-resolution approximations to the latter take the balloon-like shapes visible in figure 1. The most profound feature of both spectra in figure 1 is that all leading eigenvalues have positive real parts, indicating the presence of a linear instability. Surprisingly, two of the three leading eigenvalues in pPF have numerically almost identical real parts for all values of the parameters we considered (see also figure 6 below).

To demonstrate numerical convergence, in figure 1 we present the eigenvalue spectra for two spectral resolutions, with $M = 50$ and $M = 100$ Chebyshev polynomials, respectively, and observe that the physical eigenvalues are well-converged. All calculations presented below are therefore carried out with $M = 50$. While this spectral resolution is quite low to yield converged results in the no-slip setting (Wilson *et al.* 1999; Khalid *et al.* 2021*b*), it is clearly sufficient for the free-slip boundary conditions. This observation supports our original rationale that the free-slip boundary conditions simplify numerical simulations of such flows by removing steep near-wall velocity gradients.

For no-slip boundary conditions, the least stable eigenmode of pCF and one of the three leading eigenmodes of pPF are mostly localised in the vicinity of the confining boundaries (Gorodtsov & Leonov 1967; Wilson *et al.* 1999), and are thus referred to as *wall modes*, while the other two pPF modes are mostly localised in the bulk (Wilson *et al.* 1999; Khalid *et al.* 2021*b*), i.e. they are *centre modes*. In figure 2 we present the spatial profiles corresponding to the unstable free-slip eigenvalues discussed above, and observe

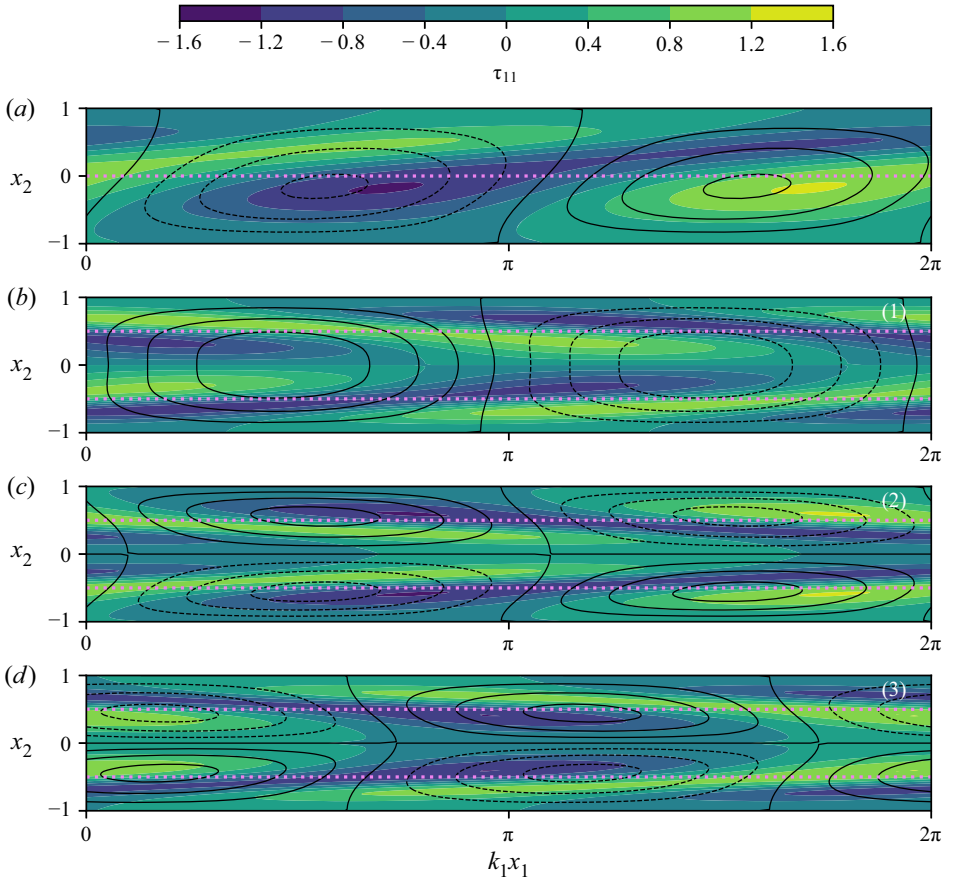

Figure 2. Spatial profiles of the polymeric stress $\delta\tau_{11}$ (colour) and the streamfunction (contours with negative values denoted by dashed lines) corresponding to the unstable eigenvalues in figure 1 for $\beta = 0.1$ and $k_1 = 0.65$: (*a*) pCF at $Wi = 2.5$; (*b*)–(*d*) pPF eigenmodes (1)–(3) at $Wi = 4.0$ (see figure 1*b*). The violet dotted lines denote the positions of the maxima of the base components $|\tau_{12}|$ and $|\tau_{11}|$.

that the distinction between wall and centre mode is significantly weakened. Although the symmetries of the stress distribution and the streamfunction are still different between these modes (compare the vortex structure in figure 2(*a*,*b*) with (*c*,*d*), for instance), all modes now have significant presence throughout the domain. Notably, the fact that all these modes can be simultaneously unstable indicates the presence of several, rather different instability mechanisms.

In figure 3 we present the neutral stability curves for various values of β, while figure 4 shows the critical Weissenberg number Wi_c and the corresponding critical wavenumber $k_{1,c}$ as functions of β. The neutral stability curves are skewed towards small values of k_1 in a way reminiscent of the elasto-inertial (Chaudhary *et al.* 2019; Khalid *et al.* 2021*a*) and purely elastic modes (Khalid *et al.* 2021*b*) discovered recently. Despite these similarities, we were unable to use the re-scaling procedure proposed in those works to collapse all our neutral stability data on a single master curve. Furthermore, in figure 4(*a*) we observe that Wi_c increases rapidly as $\beta \to 1$, indicating that a sufficiently strong velocity–stress coupling is required to drive the instability. We also note that Wi_c is significantly smaller for pPF than for pCF, and that, surprisingly, the critical wavenumber $k_{1,c}$ depends in

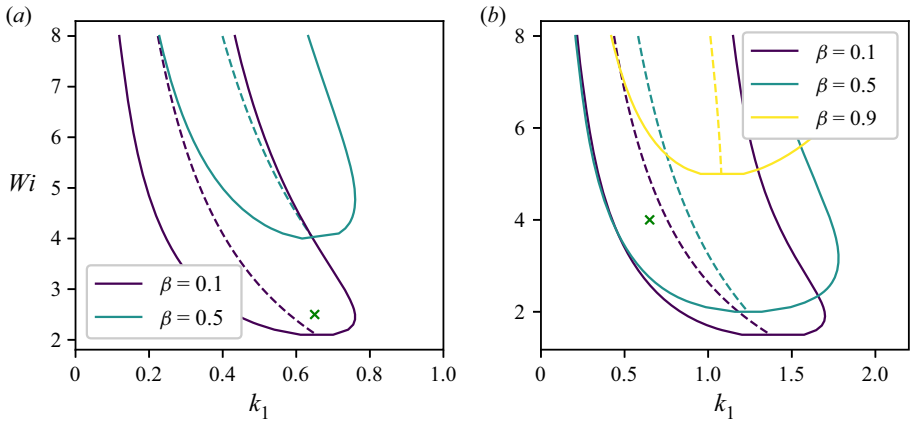

Figure 3. Neutral stability curves (solid lines) and the positions of the most unstable eigenvalue maxima (dashed lines) for (*a*) pCF and (*b*) pPF. The green crosses correspond to the parameters used in figure 1.

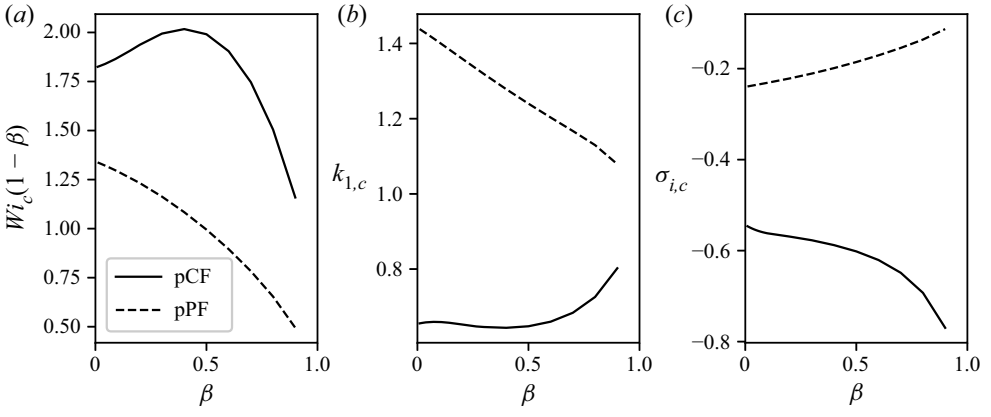

Figure 4. (*a*) The critical Weissenberg number Wi_c as a function of β. (*b*) The corresponding critical wavenumber $k_{1,c}$, and (*c*) the imaginary part of the critical eigenvalue $\sigma_{i,c}$, as a function of β.

different ways on β for these flows. As can be seen in figure 4(*b*), in all cases, $k_{1,c} \sim O(1)$, indicating an instability length scale comparable with the wall-to-wall distance.

To assess the influence of weak inertia, in figure 5 we plot the leading eigenvalue of pCF and pPF as a function of the Reynolds number. We see that while small amounts of inertia have a stabilising effect on pCF, the low-β instabilities in pPF are only mildly suppressed. For pPF at sufficiently high β, the trend reverses, and we observe a stable purely elastic eigenmode becoming unstable for $Re > 0$. While a full $Wi - \beta - Re$ critical surface is required to draw a definite conclusion regarding the influence of inertia on each mode, we note here that our observations are in line with the recent work on elasto-inertial instabilities (Chaudhary *et al.* 2019; Khalid *et al.* 2021*a*).

The spectra presented in figure 1 bear a striking resemblance to the spectra of the corresponding flows of Oldroyd-B fluids with no-slip boundary conditions (Gorodtsov & Leonov 1967; Wilson *et al.* 1999) but for the position of the leading eigenvalues, which appear to move to positive values of σ_r in the free-slip case. To establish a connection between these eigenvalues and their no-slip counterparts, we perform a homotopy between the two types of boundary conditions. To this end, we introduce a laminar profile that

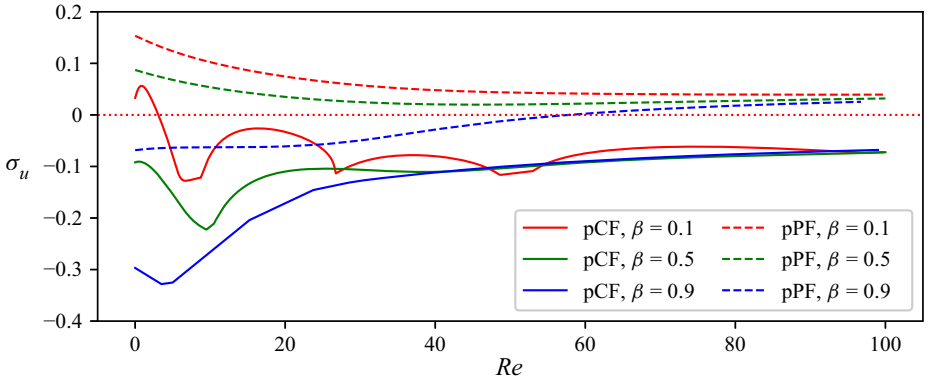

Figure 5. Influence of weak inertia on linear instability of pCF and pPF at $Wi = 2.5$ and $Wi = 4.0$, respectively, at $k_1 = 0.65$ as denoted by the green cross in figure 3. The dotted red line denotes marginal stability.

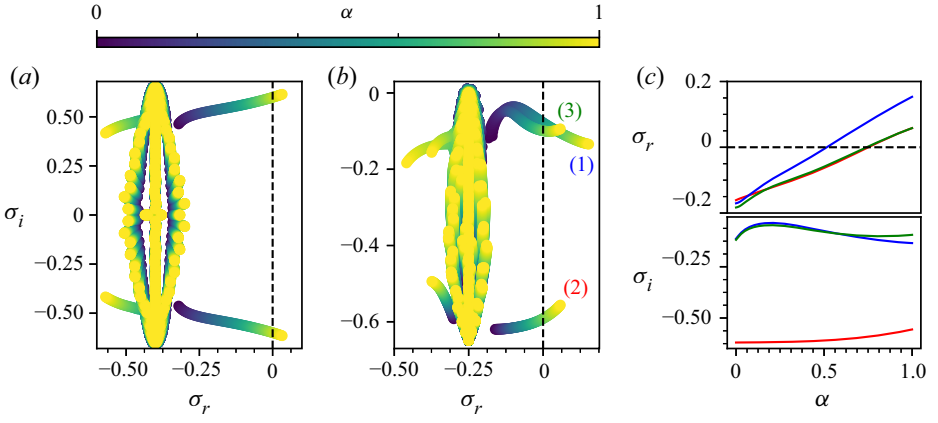

Figure 6. (*a*,*b*) Eigenvalue spectrum of system with continuously varied boundary conditions from free-slip (yellow) to no-slip (violet) for (*a*) pCF at $Wi = 2.5$ and (*b*) pPF at $Wi = 4.0$. Data shown in both panels were calculated for $\beta = 0.1$, $Re = 0.0$ and $k_1 = 0.65$. The black dashed line denotes marginal stability. Each spectrum is colour-coded according to the value of the homotopy parameter α. (*c*) Real and imaginary parts of the three leading eigenvalues from (*b*) as a function of α. The dashed line denotes the instability threshold. The leading pCF eigenvalues (not shown) become stable for $\alpha < 0.88$, while the leading pPF eigenvalues (1), (2) and (3) become stable for $\alpha < 0.52$, 0.75 and 0.74, respectively.

depends on a parameter α,

$$U(x_2) = \begin{cases} \alpha \sin(\pi x_2/2) + (1-\alpha)x_2 & (\text{pCF}), \\ \alpha \cos(\pi x_2/2)^2 + (1-\alpha)(1-x_2^2) & (\text{pPF}), \end{cases} \tag{3.1}$$

which interpolates between (2.3) ($\alpha = 1$) and the classical no-slip pCF and pPF profiles ($\alpha = 0$). A similar interpolation is imposed on the boundary conditions:

$$\alpha \partial_2 \delta v_1 \pm (1-\alpha)\delta v_1 = v_2 = \alpha \partial_2 \delta v_3 \pm (1-\alpha)\delta v_3 = 0, \quad \text{for } x_2 = \pm 1. \tag{3.2}$$

In figure 6 we show the superimposed spectra for this laminar profile as a function of α for pCF and pPF. The results of the homotopy procedure clearly indicate that the unstable modes do not appear either from infinity or from the continuous spectra, but instead are

continuously connected to the well-known least stable eigenvalues of no-slip parallel shear flows (Gorodtsov & Leonov 1967; Wilson *et al.* 1999).

4. Conclusions

In this work, we demonstrate that free-slip pCF and pPF of Oldroyd-B fluids are linearly unstable. The instabilities we observe are caused neither by the curvature of the base flow streamlines, where hoop stresses are known to lead to purely elastic instabilities (McKinley, Pakdel & Öztekin 1996), nor by steep gradients of the material properties, as in the co-extrusion problems (Hinch, Harris & Rallison 1992). Suggestively, the base velocity profiles considered here change the sign of their second derivatives inside the domain, which might indicate a connection to Rayleigh's inflection point instability criterion for inviscid fluids (Drazin & Reid 2004). A similar situation occurs in purely elastic Kolmogorov flows (Boffetta *et al.* 2005), and it would be interesting to examine whether the instabilities observed there are related to those found in this work. By performing a homotopy between free-slip and no-slip boundary conditions, we demonstrate that the unstable eigenmodes are directly related to the least stable modes of the no-slip system. The exact way by which the introduction of an inflection point into the base profile would lead to destabilisation of the no-slip modes is currently unknown.

While the body forcing and the boundary conditions considered here are probably difficult, if not impossible, to realise in practice, the main importance of our work is not related to its direct experimental relevance. Instead, our contribution here is related to the observation that the free-slip problem considered here is significantly simpler to address numerically than its no-slip counterpart. Even at the linear level, a significantly lower number of Chebyshev modes is needed to resolve the eigenspectrum than in the no-slip case. A similar simplification is also expected to occur in fully nonlinear direct numerical simulations and to alleviate the high Weissenberg number problem plaguing such studies. By rendering the leading eigenmodes unstable, free-slip flows offer an easier route to the study of strongly sub-critical structures that propagate from those eigenmodes in the no-slip case (Morozov & van Saarloos 2005, 2007, 2019).

Once coherent states are resolved in direct numerical simulations of free-slip flows, a boundary condition homotopy similar to the one employed here can be used to track those solutions back to the no-slip conditions (Waleffe 2003). Recent work on elasto-inertial parallel shear flows (Garg *et al.* 2018; Chaudhary *et al.* 2019, 2021; Khalid *et al.* 2021*a*) associates linear instabilities at high Wi and Re with the very leading eigenvalues studied here. As already mentioned above, the same instability can be traced to the purely elastic case, $Re = 0$, for sufficiently large values of β and Wi (Khalid *et al.* 2021*b*). It has also been shown that these instabilities are sub-critical in nature (Page, Dubief & Kerswell 2020). Taken together with the original proposal of Morozov & van Saarloos (2005, 2007, 2019) and the experimental and numerical studies of nonlinear states in elasto-inertial flows (Dubief, Terrapon & Soria 2013; Samanta *et al.* 2013; Choueiri, Lopez & Hof 2018; Sid, Terrapon & Dubief 2018; Lopez, Choueiri & Hof 2019), this points towards the existence of exact coherent states related to the least stable eigenvalues, even though they are linearly stable for most values of β and Wi. Our work suggests using a homotopy from free-slip flows to discover these structures.

Finally, we note that our results suggest that all three leading eigenvalues of free-slip pPF can become unstable; see figure 1, for example. In elasto-inertial flows, there is an ongoing discussion whether the most dynamically relevant coherent structures are related to wall or centre-line modes (Shekar *et al.* 2019; Datta *et al.* 2021). In figure 7, we present the neutral stability curve for the first three eigenvalues and observe that by selecting the

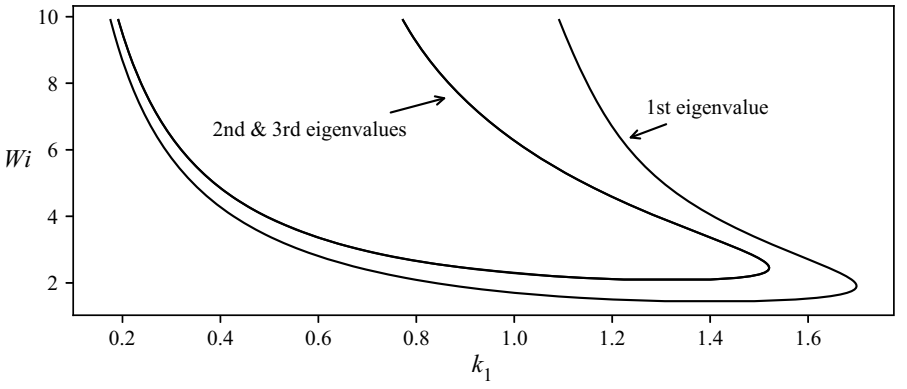

Figure 7. Neutral stability curves of the first three eigenvalues of pPF for $\beta = 0.1$. As mentioned in § 3, the second and third eigenvalues have the same real parts, and their instability regions coincide.

wavenumber and the Weissenberg number, one can control the type of the instability thus produced. As figure 2 suggests, the different spatial symmetries of those modes should result in structures that connect to either wall or centre-line modes, when traced back to the no-slip conditions, thus allowing one to assess their relative importance independently.

Acknowledgements. Professor Eckhardt took active part in conceiving this project and interpreting the free-slip plane Couette flow results. He did not see the part of this work on plane Poiseuille flow, which we hope we continued in line with his high scientific standards. All shortcomings should be attributed to A.M.

Declaration of interest. The authors report no conflict of interest.

Author ORCIDs.
Moritz Linkmann https://orcid.org/0000-0002-3394-1443;
Bruno Eckhardt https://orcid.org/0000-0003-4050-3254;
Alexander Morozov https://orcid.org/0000-0003-4498-3910.

References

Alves, M.A., Oliveira, P.J. & Pinho, F.T. 2021 Numerical methods for viscoelastic fluid flows. *Annu. Rev. Fluid Mech.* **53**, 509–541.

Bird, R.B., Armstrong, R.C. & Hassager, O. 1987 *Dynamics of Polymeric Liquids: Fluid Mechanics*, 2nd edn. John Wiley and Sons Inc.

Bistagnino, A., Boffetta, G., Celani, A., Mazzino, A., Puliafito, A. & Vergassola, M. 2007 Nonlinear dynamics of the viscoelastic Kolmogorov flow. *J. Fluid Mech.* **590**, 61–80.

Black, W.B. & Graham, M.D. 1996 Wall-slip and polymer-melt flow instability. *Phys. Rev. Lett.* **77**, 956–959.

Black, W.B. & Graham, M.D. 1999 Effect of wall slip on the stability of viscoelastic plane shear flow. *Phys. Fluids* **11** (7), 1749–1756.

Black, W.B. & Graham, M.D. 2001 Slip, concentration fluctuations, and flow instability in sheared polymer solutions. *Macromolecules* **34** (17), 5731–5733.

Boffetta, G., Celani, A., Mazzino, A., Puliafito, A. & Vergassola, M. 2005 The viscoelastic kolmogorov flow: eddy viscosity and linear stability. *J. Fluid Mech.* **523**, 161–170.

Bonn, D., Ingremeau, F., Amarouchene, Y. & Kellay, H. 2011 Large velocity fluctuations in small-Reynolds-number pipe flow of polymer solutions. *Phys. Rev.* E **84**, 045301.

Canuto, C., Hussaini, M.Y., Quarteroni, A. & Zang, T.A. 1987 *Spectral Methods in Fluid Dynamics*. Springer-Verlag.

Chaudhary, I., Garg, P., Shankar, V. & Subramanian, G. 2019 Elasto-inertial wall mode instabilities in viscoelastic plane poiseuille flow. *J. Fluid Mech.* **881**, 119–163.

CHAUDHARY, I., GARG, P., SUBRAMANIAN, G. & SHANKAR, V. 2021 Linear instability of viscoelastic pipe flow. *J. Fluid Mech.* **908**, A11.
CHOUEIRI, G.H., LOPEZ, J.M. & HOF, B. 2018 Exceeding the asymptotic limit of polymer drag reduction. *Phys. Rev. Lett.* **120** (12), 124501.
DATTA, S., *et al.* 2021 Perspectives on viscoelastic flow instabilities and elastic turbulence. arXiv:2108.09841.
DRAZIN, P.G. & REID, W.H. 2004 *Hydrodynamic Stability*. Cambridge University Press.
DUBIEF, Y., TERRAPON, V.E. & SORIA, J. 2013 On the mechanism of elasto-inertial turbulence. *Phys. Fluids* **25** (11), 110817.
ECKHARDT, B., SCHNEIDER, T.M., HOF, B. & WESTERWEEL, J. 2007 Turbulence transition in pipe flow. *Annu. Rev. Fluid Mech.* **39**, 447–468.
GARG, P., CHAUDHARY, I., KHALID, M., SHANKAR, V. & SUBRAMANIAN, G. 2018 Viscoelastic pipe flow is linearly unstable. *Phys. Rev. Lett.* **121** (2), 024502.
GERSTING, J.M. 1974 Hydrodynamic stability of plane porous slip flow. *Phys. Fluids* **17** (11), 2126–2127.
GORODTSOV, V.A. & LEONOV, A.I. 1967 On a linear instability of a plane parallel Couette flow of viscoelastic fluid. *Z. Angew. Math. Mech.* **31** (2), 310–319.
GRAHAM, M.D. & FLORYAN, D. 2021 Exact coherent states and the nonlinear dynamics of wall-bounded turbulent flows. *Annu. Rev. Fluid Mech.* **53**, 227–253.
GROISMAN, A. & STEINBERG, V. 2000 Elastic turbulence in a polymer solution flow. *Nature* **405** (6782), 53–55.
GROSSMANN, S. 2000 The onset of shear flow turbulence. *Rev. Mod. Phys.* **72** (2), 603–618.
HINCH, E.J., HARRIS, O.J. & RALLISON, J.M. 1992 The instability mechanism for two elastic liquids being co-extruded. *J. Non-Newtonian Fluid Mech.* **43** (2), 311–324.
KHALID, M., CHAUDHARY, I., GARG, P., SHANKAR, V. & SUBRAMANIAN, G. 2021*a* The centre-mode instability of viscoelastic plane Poiseuille flow. *J. Fluid Mech.* **915**, A43.
KHALID, M., SHANKAR, V. & SUBRAMANIAN, G. 2021*b* A continuous pathway between the elasto-inertial and elastic turbulent states in viscoelastic channel flow. *Phys. Rev. Lett.* **127** (13), 134502.
LAUGA, E. & COSSU, C. 2005 A note on the stability of slip channel flows. *Phys. Fluids* **17** (8), 088106.
LOPEZ, J.M., CHOUEIRI, G.H. & HOF, B. 2019 Dynamics of viscoelastic pipe flow at low Reynolds numbers in the maximum drag reduction limit. *J. Fluid Mech.* **874**, 699–719.
MCKINLEY, G.H., PAKDEL, P. & ÖZTEKIN, A. 1996 Rheological and geometric scaling of purely elastic flow instabilities. *J. Non-Newtonian Fluid Mech.* **67**, 19–47.
MIN, T. & KIM, J. 2005 Effects of hydrophobic surface on stability and transition. *Phys. Fluids* **17** (10), 108106.
MOROZOV, A. & VAN SAARLOOS, W. 2019 Subcritical instabilities in plane poiseuille flow of an oldroyd-b fluid. *J. Stat. Phys.* **175** (3), 554–577.
MOROZOV, A.N. & VAN SAARLOOS, W. 2005 Subcritical finite-amplitude solutions for plane Couette flow of viscoelastic fluids. *Phys. Rev. Lett.* **95** (2), 024501.
MOROZOV, A.N. & VAN SAARLOOS, W. 2007 An introductory essay on subcritical instabilities and the transition to turbulence in visco-elastic parallel shear flows. *Phys. Rep.* **447** (3-6), 112–143.
OWENS, R.G. & PHILLIPS, T.N. 2002 *Computational Rheology*. World Scientific.
PAGE, J., DUBIEF, Y. & KERSWELL, R.R. 2020 Exact traveling wave solutions in viscoelastic channel flow. *Phys. Rev. Lett.* **125** (15), 154501.
PAN, L., MOROZOV, A., WAGNER, C. & ARRATIA, P.E. 2013 Nonlinear elastic instability in channel flows at low Reynolds numbers. *Phys. Rev. Lett.* **110** (17), 174502.
QIN, B. & ARRATIA, P.E. 2017 Characterizing elastic turbulence in channel flows at low Reynolds number. *Phys. Rev. Lett.* **2** (8), 083302.
RAYLEIGH, LORD 1916 On convection currents in a horizontal layer of fluid, when the higher temperature is on the under side. *Lond. Edinb. Dublin Philos. Mag. J. Sci.* **32** (192), 529–546.
SAMANTA, D., DUBIEF, Y., HOLZNER, M., SCHÄFER, C., MOROZOV, A.N., WAGNER, C. & HOF, B. 2013 Elasto-inertial turbulence. *Proc. Natl Acad. Sci. USA* **110** (26), 10557–10562.
SHEKAR, A., MCMULLEN, R.M., WANG, S.-N., MCKEON, B.J. & GRAHAM, M.D. 2019 Critical-layer structures and mechanisms in elastoinertial turbulence. *Phys. Rev. Lett.* **122**, 124503.
SID, S., TERRAPON, V.E. & DUBIEF, Y. 2018 Two-dimensional dynamics of elasto-inertial turbulence and its role in polymer drag reduction. *Phys. Rev. Fluids* **3**, 011301.
STEINBERG, V. 2021 Elastic turbulence: an experimental view on inertialess random flow. *Annu. Rev. Fluid Mech.* **53**, 27–58.
TUCKERMAN, L.S., CHANTRY, M. & BARKLEY, D. 2020 Patterns in wall-bounded shear flows. *Annu. Rev. Fluid Mech.* **52**, 343–367.

VIRTANEN, P., *et al.* 2020 SciPy 1.0: fundamental algorithms for scientific computing in python. *Nat. Meth.* **17**, 261–272.

WALEFFE, F. 1997 On a self-sustaining process in shear flows. *Phys. Fluids* **9** (4), 883–900.

WALEFFE, F. 2003 Homotopy of exact coherent structures in plane shear flows. *Phys. Fluids* **15** (6), 1517–1534.

WILSON, H.J., RENARDY, M. & RENARDY, Y. 1999 Structure of the spectrum in zero Reynolds number shear flow of the ucm and oldroyd-b liquids. *J. Non-Newtonian Fluid Mech.* **80** (2–3), 251–268.